# CARBON BASED SMART SYSTEM FOR WIRELESS APPLICATION


**Start Date : 01/09/12**
**Project n°318352** **Duration : 36 months**

**Topic addressed : Very advanced nanoelectronic components: design, engineering, technology and manufacturability**

## WORK PACKAGE 6 : Dissemination and exploitation activities

# DELIVERABLE D6.4

# Publication of e-newsletter #3

**Due date : T0+36** **Submission date : T0+37**

**Lead contractor for this deliverable : TRT**

**Dissemination level : PU – Public**

WORK PACKAGE 6: Dissemination and exploitation activities

**PARTNERS ORGANISATION APPROVAL**

| | Name | Function | Date | Signature |
|---|---|---|---|---|
| Prepared by: | S.Xavier | R&D Engineer | 29/10/15 | |
| Approved by: | Afshin Ziaei | Research Program Manager | 29/10/15 | |

# DISTRIBUTION LIST

| QUANTITY | ORGANIZATION | | NAMES |
|---|---|---|---|
| 1 ex | Thales Research and Technology | TRT | Afshin ZIAEI |
| 1 ex | Chalmers University of Technology | CHALMERS | Johan LIU |
| 1 ex | Foundation for Research & Technology - Hellas | FORTH | George KONSTANDINIS |
| 1 ex | Laboratoire d'Architecture et d'Analyse des Systèmes | CNRS-LAAS | George DELIGEORGIS |
| 1 ex | Université Pierre et Marie Curie | UPMC | Charlotte TRIPON-CANSELIET |
| 1 ex | National Research and Development Institute for Microtechnologies | IMT | Mircea DRAGOMAN |
| 1 ex | Graphene Industries | GI | Peter BLAKE |
| 1 ex | Thales Systèmes Aéroportés | TSA | Yves MANCUSO |
| 1 ex | SHT Smart High-Tech AB | SHT | Yifeng FU |
| 1 ex | Universita politecnica delle Marche | UNIVPM | Luca PIERANTONI |
| 1 ex | Linköping University | LiU | Rositsa YAKIMOVA |
| 1 ex | Fundacio Privada Institute Catala de Nanotecnologia | ICN | Clivia SOTOMAYOR |
| 1 ex | Tyndall-UCC | Tyndall | Mircea MODREANU |

# CHANGE RECORD SHEET

| REVISION LETTER | DATE | PAGE NUMBER | DESCRIPTION |
|---|---|---|---|
| Template | 07/2013 | | |
| V1 | 29/10/2015 | 13 | Final version |
| | | | |
| | | | |


Nano-RF is a European project and the main concept is the development of CNT & graphene based advanced component technologies for the implementation of miniaturized electronic systems for 2020 and beyond wireless communications and radars.
The developed components and technologies developed during the project will be implemented in the following *demonstrators*:

- Reflect array antennae for wake vortex and weather radars
- Graphene receiver module

The demonstrators will exhibit the reconfigurability, systemability, integratability and manufacturability of the developed technologies and unify advanced More-than-Moore elements and Beyond-CMOS devices with existing technologies. It addresses "System Perspective" to support miniaturized electronic systems for 2020 and beyond.
This Nano-RF newsletter intends to present the latest progress obtained during first year of the project.

## Design and Simulation activities

### ➢ Development of a full self-consistent Dirac-Poisson simulator for i) graphene/GNR FET, ii) GNR circuits

In case of graphene nanoribbons, the quantum transport is described by the Schroedinger equation. The Dirac equation can be applied to 2D graphene.

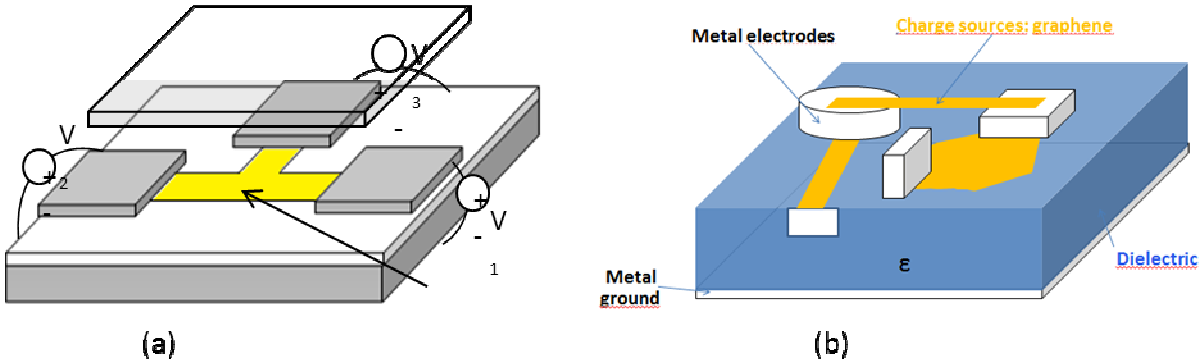


**Figure 1 : General GNR-FET like device (a), with, possibly, many ports for charge injection; full 3D Poisson solver: typical configuration (b).**

As depicted in Figure 1 (a), many branches and ports GNR-devices are simulated by our developed solver, with a wide variety of possible applications, e.g.: multiport GNR circuits, scattering by lattice defects, change in width in cascade GNRs, crossing GNRs, T-junctions, metal-carbon contact, field coupling among GNRs. Moreover, a novel, optimized full-3D Poisson solver has been recently developed and inserted in the main code. It is possible to deal with realistic 3D devices with high geometrical/electrical aspect ratios, involving: ground planes, metal electrodes, charge sources (graphene/CNT) etc. (Figure 1(b)). The shape of electrodes can be arbitrary, as well as the shape of (2D-3D) charge sources.
As for the CNT-FET, the Schrödinger equation is written for each individual transport channel of a GNR channel

$$\frac{d^2\Psi_{h,e}^{n,m}}{dz^2} = -\frac{2m_{h,e}^{n,m}}{\hbar^2}\left(E - U_{h,e}^{n,m}(z)\right)\Psi_{h,e}^{n,m}$$

where V is the electrostatic potential satisfying the Poisson equation

However, for the GNR-FET the analysis is: i) 3D for the potential (no geometrical symmetry), ii) 2D for the charge transport.
In the following example, a numerical result is reported. The simulated device is shown in Figure 2, where D is the oxide thickness and a relative dielectric constant of 25 is ideally assumed for the substrate.

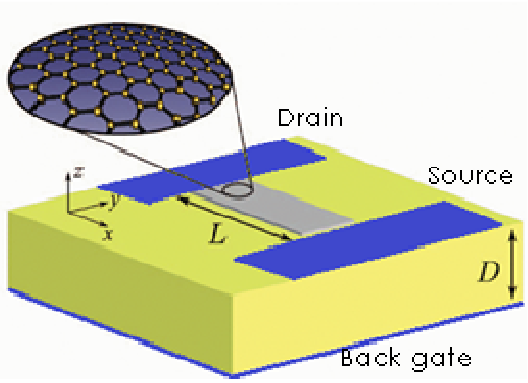


**Figure 2 : GNR-FET**

Current-voltage curves, for different gate voltages, and for different GN widths, are reported in Figure 3 and Figure 4 respectively.

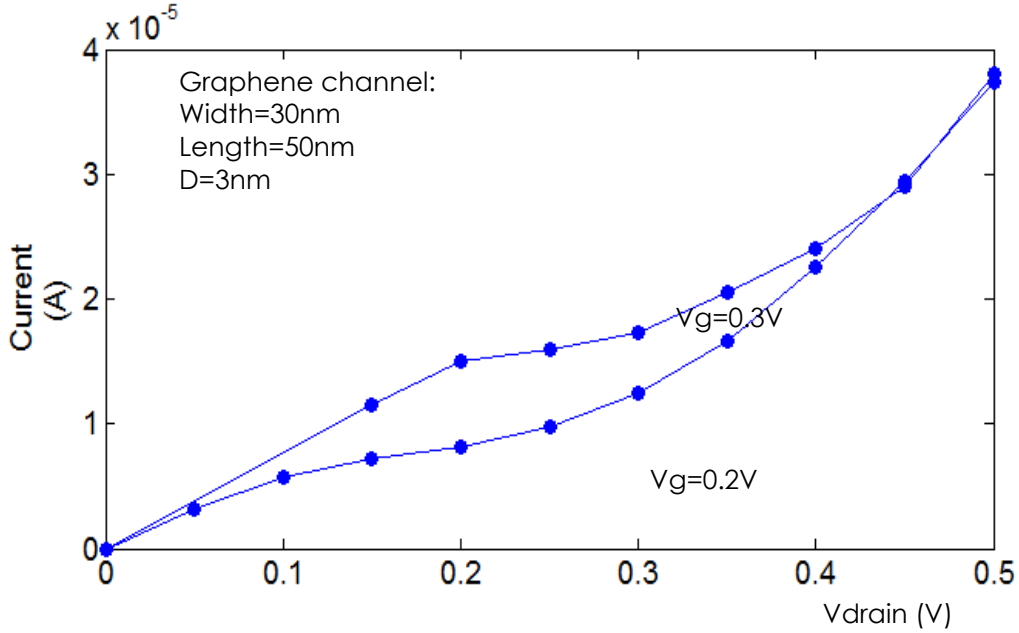


**Figure 3 : Output current vs drain voltage, for different gate voltages.**

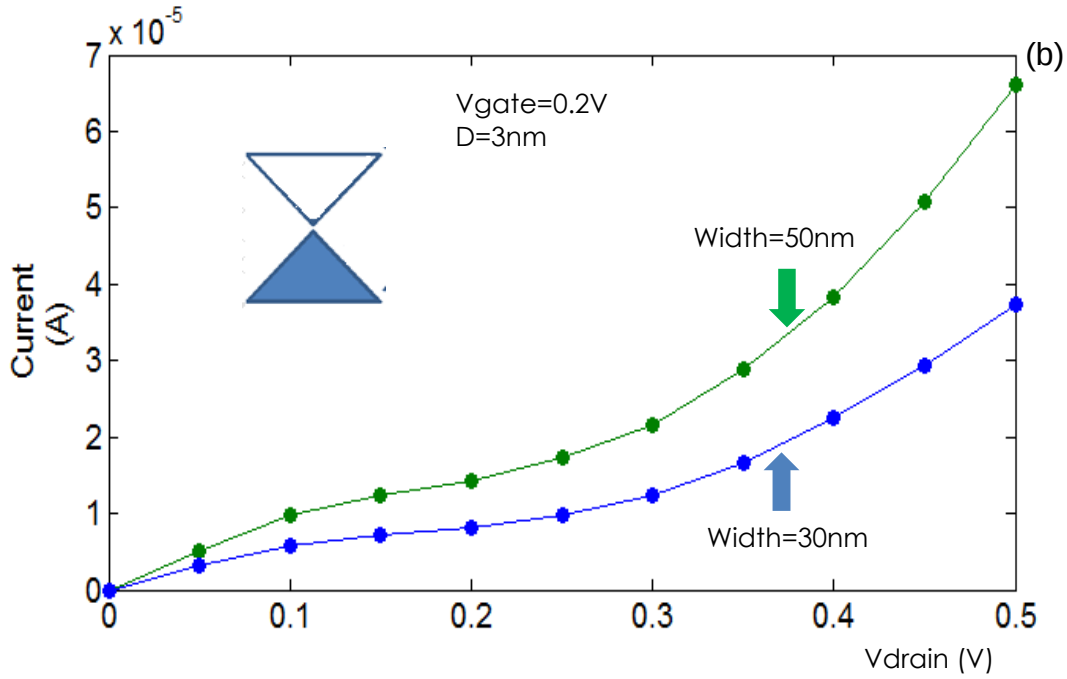


**Figure 4 : Output current vs drain voltage, for different GNR widths.**

As a result, the I-V characteristic tends to be more and more linear as the width increases, but still there is a sort of reminiscence of band gap, due to the vanishing of energy states of graphene at the Dirac point.

## ➢ Graphene FET

The geometry of the simulated graphene-FET is shown in Fig. 15: the transistor is considered as uniform in the x direction. In this case, many electrons can be injected, at different angles, and

different energies, into the channel. Figure 16 shows transmission of charge in a direction close to the Source-to-Drain direction (precisely, at a small angle of 1°). As evident from the picture, increasing the gate voltage form 0V to 0.2V produces a strong change in the transmittivity. The output current is directly related to the transmittivity, through a double integral in the wave-number space:

$$J = (4)e\iint \frac{dk_x dk_y}{(2\pi)^2} T(dk_x dk_y) v_F \frac{k_y}{|k|} f(E, u_L)$$

$$= (4)e\iint \frac{d(E) E d\theta}{(2\pi)^2 (\hbar v_F)^2} T(E, \theta) v_F \cos\theta f(E, u_L)$$

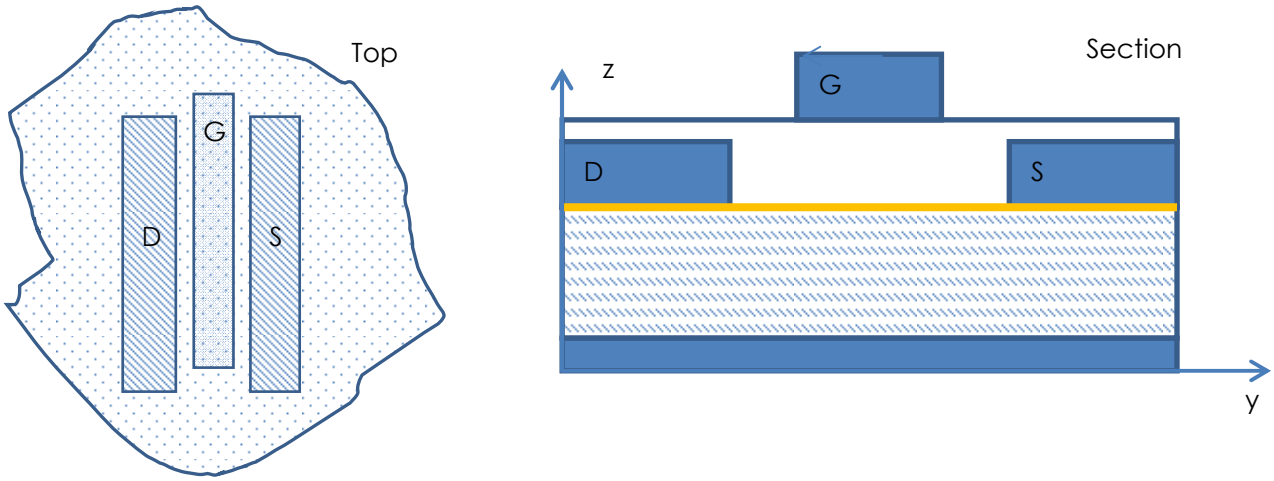


**Fig. 15.** Graphene-FET geometry.

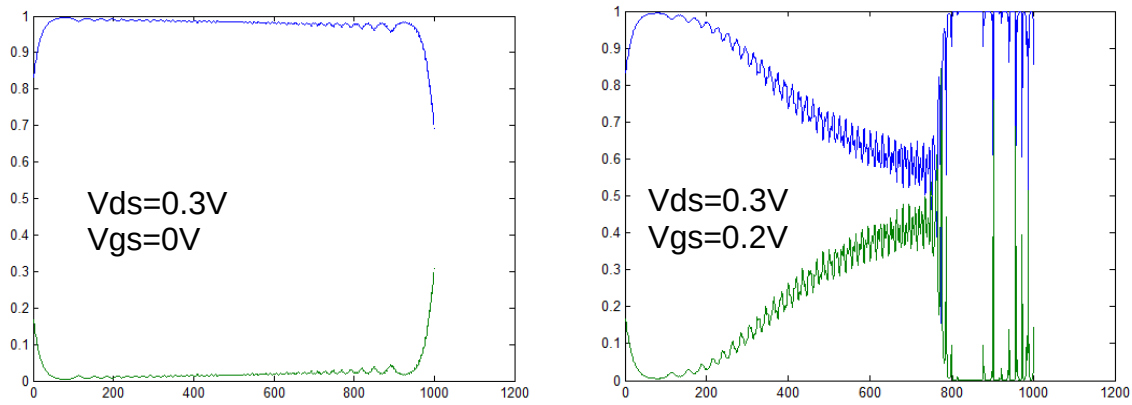


**Fig. 16.** Increasing the gate voltage, the charge transmittivity increases (green) and reflectivity reduces (blue).

The above calculation is preliminary to the final analysis of the I-V characteristic of the graphene transistor. To this aim, the fabrication data (geometry, material) are being exchanged with FORTH, and parametric analysis is presently being performed.

In order to give an idea of typical Current-Voltage characteristics for the graphene-FET, some simulated curves are reported in Fig. 17. In these examples, no self-consistency is applied. More detailed simulations, related to actually fabricated devices, are in progress.

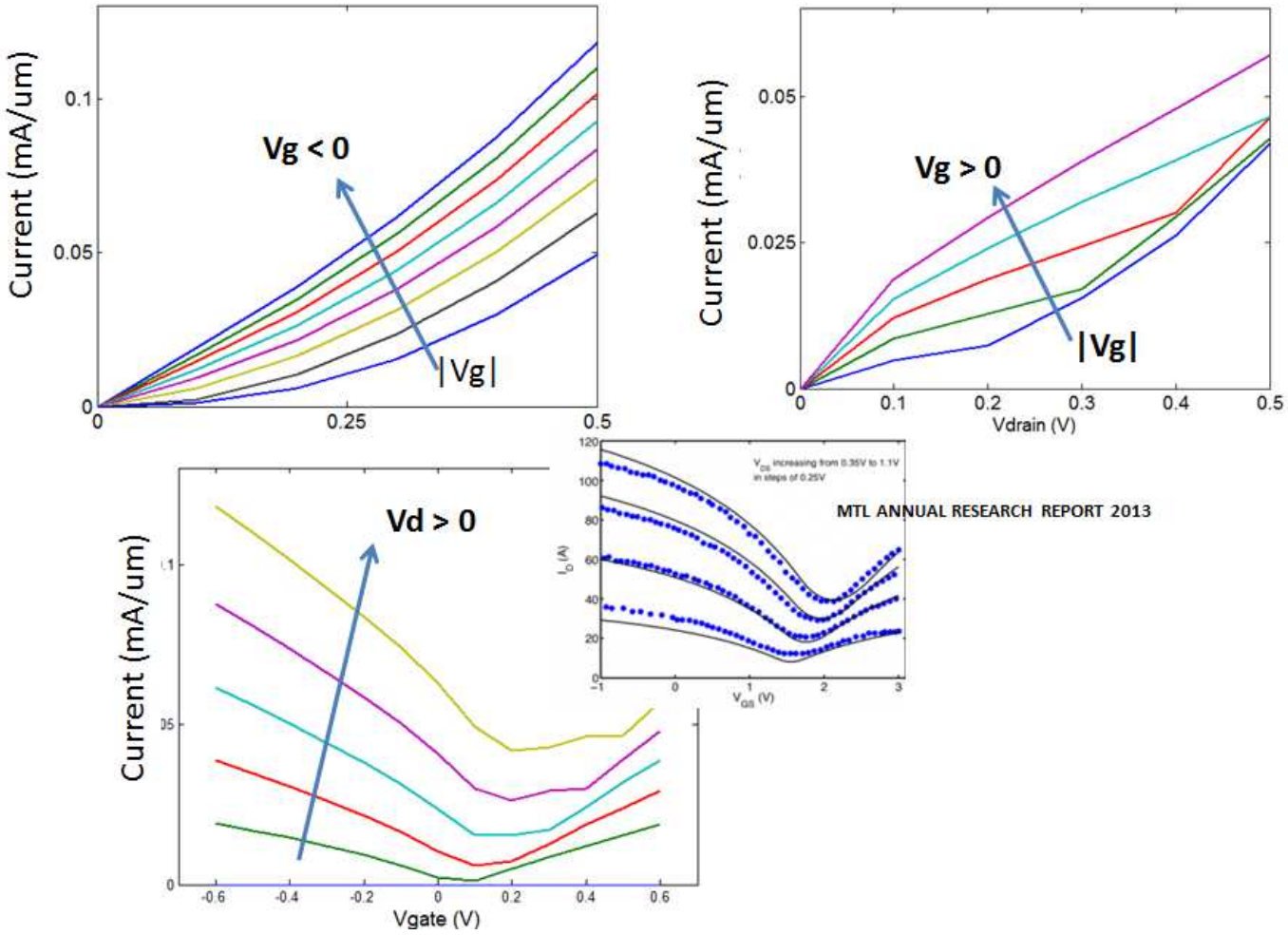


**Fig. 17.** Graphene-FET: current-voltage curves. The inset shows curves from the literature, for qualitative comparison.

# Fabrication and Test activities

## ➢ CNTs devices fabrication and characterization

### • CNT Filter

Following the design, first CNTs filter has been fabricated. On Figure 5, we can see the structure realized after CNTs growth. The different technical step was optimized to be overcome the fabrication constraints.

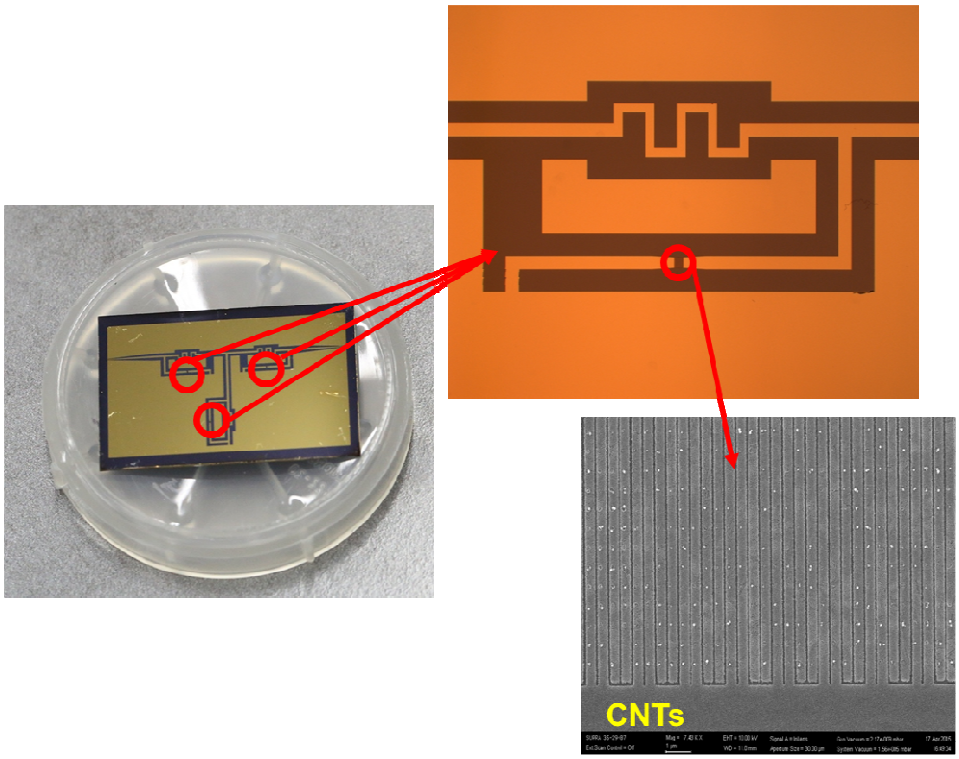


**Figure 5 : First fabrication of CNT filter**

The result of the preliminary measurement is presented Figure 6

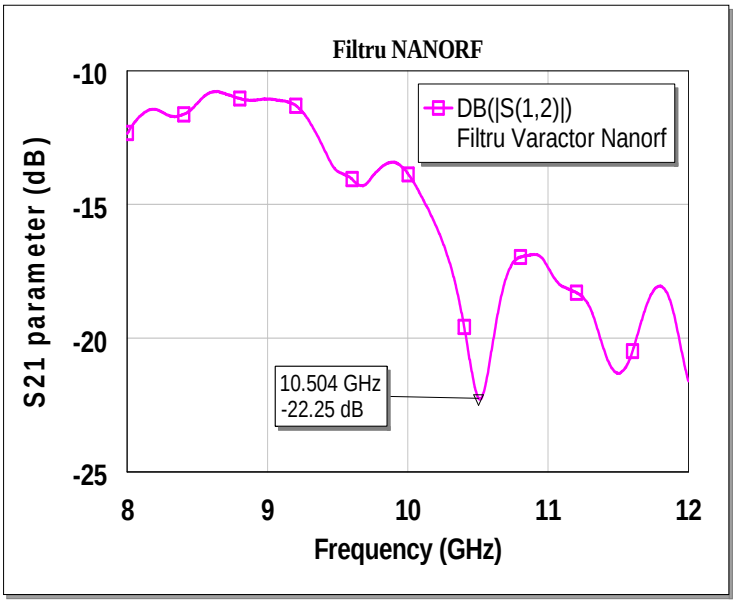


**Figure 6 : CNT filter mea surement**

The result of the measurement validates the design and the technological process. The filter two terminals fit with probe tips of 150 microns pitch and we were able to measure the filter. The molybdenum deposition is compatible with the filter.
Measurements shows filter resonance at 10 GHz which is compatible with the specification and losses due to Mo

The CNT are shorter than required, they are missing in many points. You cannot actuate them. For the next run a special attention to CNT growth is necessary.

- CNTs FET

By upgrading the CVD system, one top heater is added to minimize the thermal gradient around the sample as shown in Figure 7(a). In the meantime, the top heater can warm the gases when they flow through the shower head. In order to increase the density of horizontal SWCNT, the chamber pressure was adjusted to enhance the activity of nano-particles (catalyst) as shown in Figure 7(b).

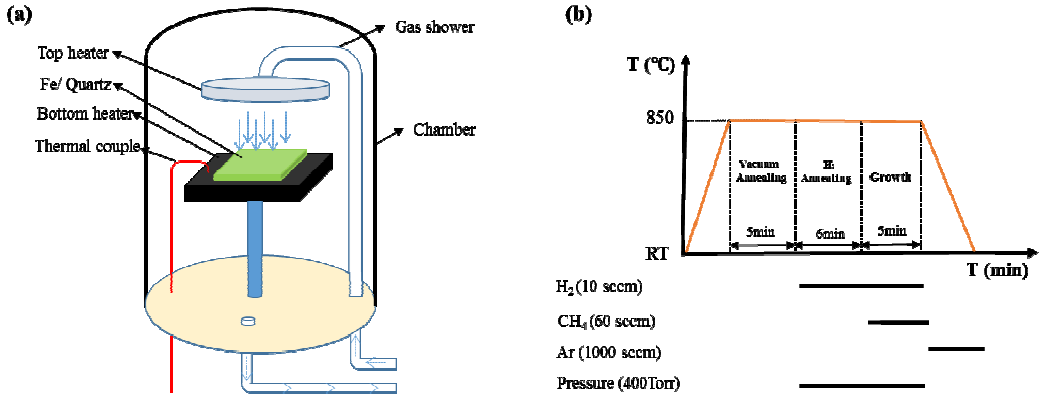


**Figure 7 : (a) Schematic of upgraded CVD system (b) optimized recipe for 0.2nm Fe sample**

It was found that the density is dependent on the chamber pressure during the growth. Thicker catalyst tends to get high density of SWCNTs at higher chamber pressure as shown in Figure 8.

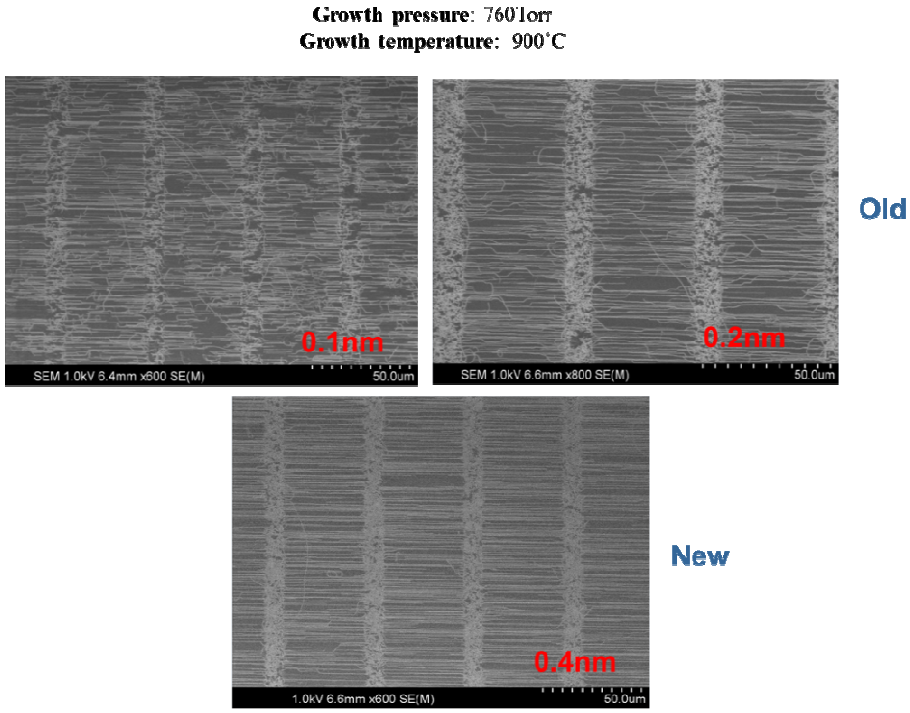


**Figure 8 : SEM of HSWCNT synthesized of 760Torr with growth temperature 900℃.**

While thinner catalyst prefers moderate chamber pressure as shown in Figure 9.

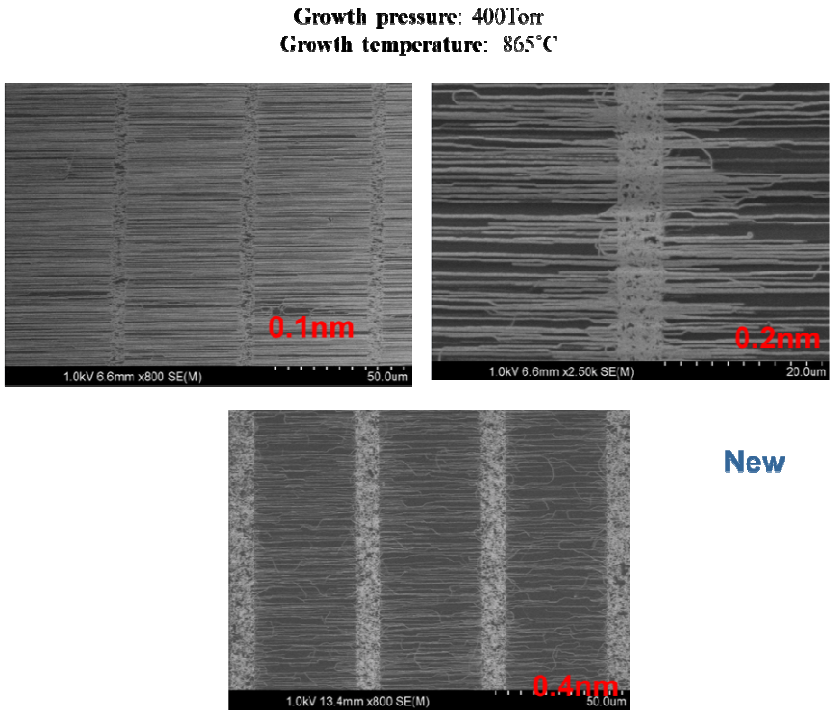


**Figure 9 : SEM of HSWCNT synthesized of 400Torr with growth temperature 865℃.**

AFM characterization has been conducted to check the specific density of pristine horizontal SWCNT on quartz substrate. It can be seen from Figure 10 that the local density of sample 1 (0.1nm) in figure 4 is highly up to 10 tubes per µm.

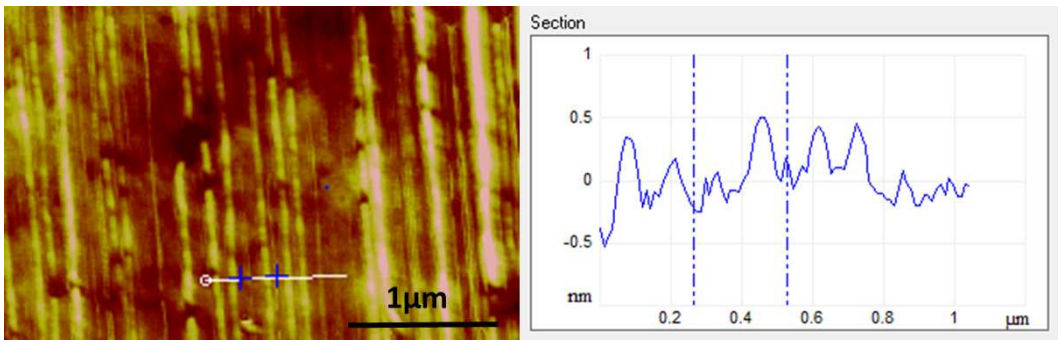


**Figure 10 : Morphology of pristine horizontal single wall CNT on quartz scanned by AFM**

- **CNTs antenna**

Following the design, first CNTs antenna has been fabricated. On Figure 11a, we can see the structure realized before CNTs growth. Technological processes matching with expected antenna design have to be overcome, as CNT diameter-to-length ratio is critical (Figure 11b). Some process procedure and design modifications are under work to overcome fabrication constraints.

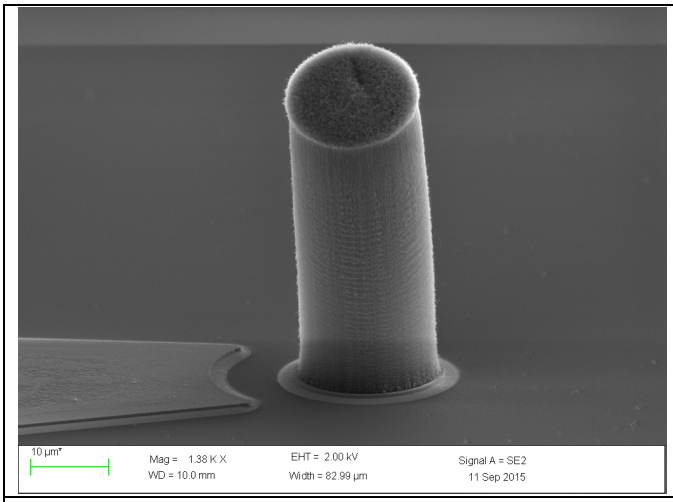


(a)

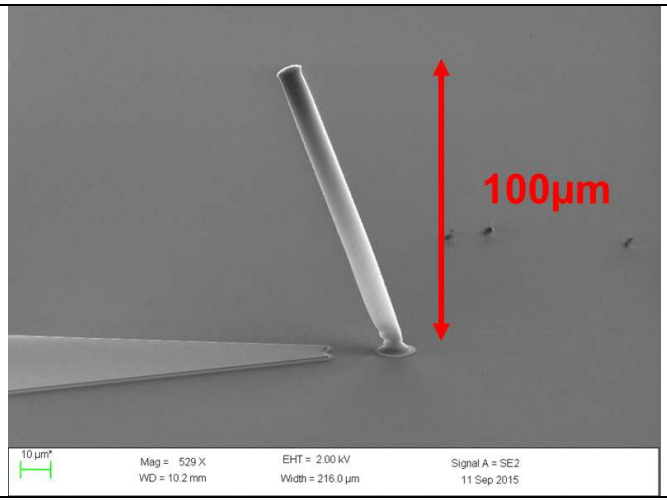


(b)

**Figure 11 : CNTs antenna fabrication and growth**

## ➢ Graphene devices fabrication and characterization

### • Graphene Growth

There are several ways to obtain graphene material and we started to study the different graphene synthesis methods.

- **Graphene CVD growth on metals**

In this period, we have tried to use a new catalyst to grow graphene by thermal chemical vapor deposition (TCVD) method. Pt-Cu alloy has been selected as the new catalyst since Cu enables uniform mono-layer graphene growth and Pt brings very large grain size of graphene. Figure 12a show the growth profile of the CVD method. Figure 12b shows the Pt-Cu alloy after growth, in which the winkles are associated with the thermal expansion coefficient difference between Pt-Cu alloy and graphene.

(a)

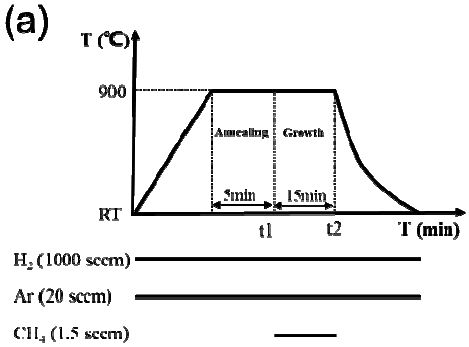


(b)

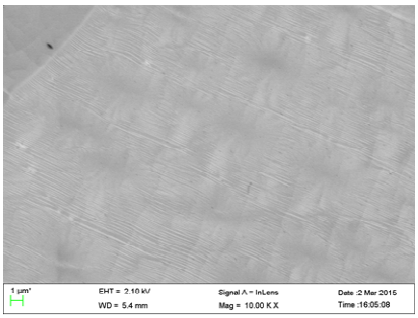

- **Figure 12. (a) Growth profile of the CVD method; (b) Pt-Cu alloy after growth.**

After growth, bubbling transfer method were used to transfer graphene from the alloy surface to Si/SiO2 substrate. **Figure 13**a shows the optical image of synthesized graphene on Si/SiO2 substrate, the blue arrows show the edge of graphene. **Figure 13**b shows the Raman spectrum of graphene after transfer process. As shown in **Figure 13**b, the intensity ratio of 2D to G higher than 2, indicating the obtained graphene is monolayer. Moreover, the low D peak indicates the high quality of the graphene.

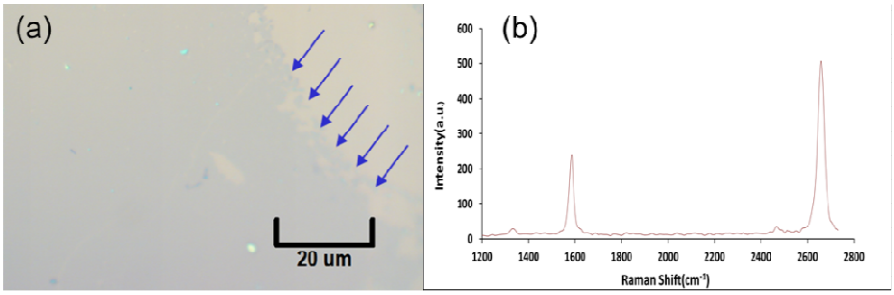


**Figure 13. (a)Optical and (b) Raman spectrum of as synthesized graphene after being transferred onto a Si with 300 nm SiO2 substrate**

In the future, electrical characterization will be carried out to further examine the graphene quality.

- **SiC decomposition**

Based on work aims of LiU in Nano RF project, we have explored the role of buffer layer and growth parameters for having a full control on the epitaxial graphene growth process on SiC to obtain cm scale continuous coverage of monolayer graphene (MLG). During the graphene growth process on the Si-face of SiC the first grown carbon layer, is covalently bonded to the SiC substrate. This so-called buffer layer lacks the π bands of graphene and only the second carbon layer (known as monolayer graphene (ML)) shows the properties of graphene. The buffer layer is a precursor for graphene formation and can strongly influence its quality; depending on the buffer layer integrity the graphene may contain defects which may work as scattering centers for carriers and decrease their mobility.

Graphene samples were grown on the Si face of different SiC polytypes in an inductively heated furnace at a temperature ranging from 1700 - 1950℃ and at argon ambient with a pressure range from 750 - 950 mbar at different growth times. Graphene surface morphology, thickness, structure and electronic properties have been assessed by using AFM, LEEM, Reflection map, Raman spectroscopy, and EFM respectively.

To improve the uniformity of the growth process and access to large scale growth up to 4 inch (**Erreur ! Source du renvoi introuvable.**), besides the excising growth cell we have made graphene growth in the recently constructed growth set-up which has some beneficial characteristics. The new system is fully automatic and just need a growth recipe to start and end up the growth process without any operator. It has also longer RF-coil with uniform distance between the pipes and also the possibility to move coil up and down to change the temperature gradient for both etching the SiC substrates and epitaxial graphene growth.

- **Figure 14 : Newly operated 4 inch growth system.**

## Graphene FET

To test and optimize the HfO2 stack deposited on the FET transistors, two fabrication runs were realized. One is a metal insulator metal structure (MIM) using Pt electrodes and the entire stack (both e-gun and ALD deposited $HfO_2$) and the second one was a Graphene insulator metal structure (GIM) resembling the actual gate structure.

For the initial MIM structures, a series of varying high-k thickness $HfO_2$ layer with thickness of 5, 10 and 15nm has been realised on a Pt continuous layer covered with a thin (1.5-2nm) layer of $HfO_2$ used for ALD nucleation. The structure was completed by a top Pt electrode. The leakage current as a function of Voltage between the top and bottom electrode has been measured and is depicted in the following plots.

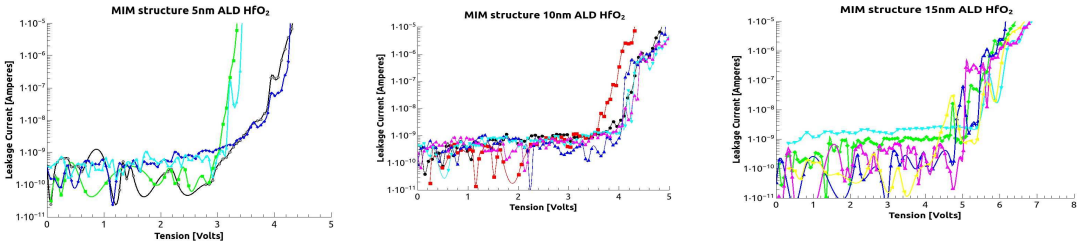


Figure 15: I-V characteristics of test MIM structures, notice the increasing breakdown voltage as the thickness of $HfO_2$ is increased from 5 to 15nm

To verify the validity of the results, a second run using graphene as the bottom electrode was realised. The top electrode was Pt and the system leakage is depicted in the following figure.

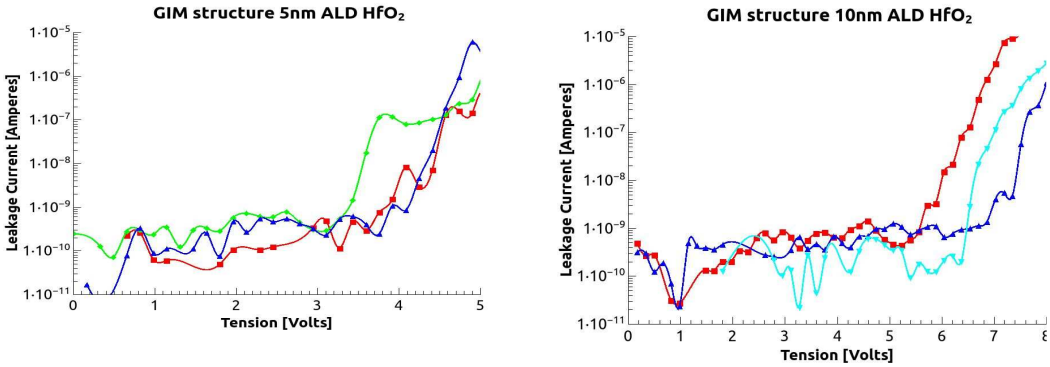


Figure 16: I-V characteristics of test GIM structures. The breakdown is larger compared to the MIM case shown in Figure 19

## Graphene Antenna

Graphene slot antenna was fabricated and initially briefly tested in the last part of 2014. The graphene antenna was fabricated on wafer and is presented in Fig.15.

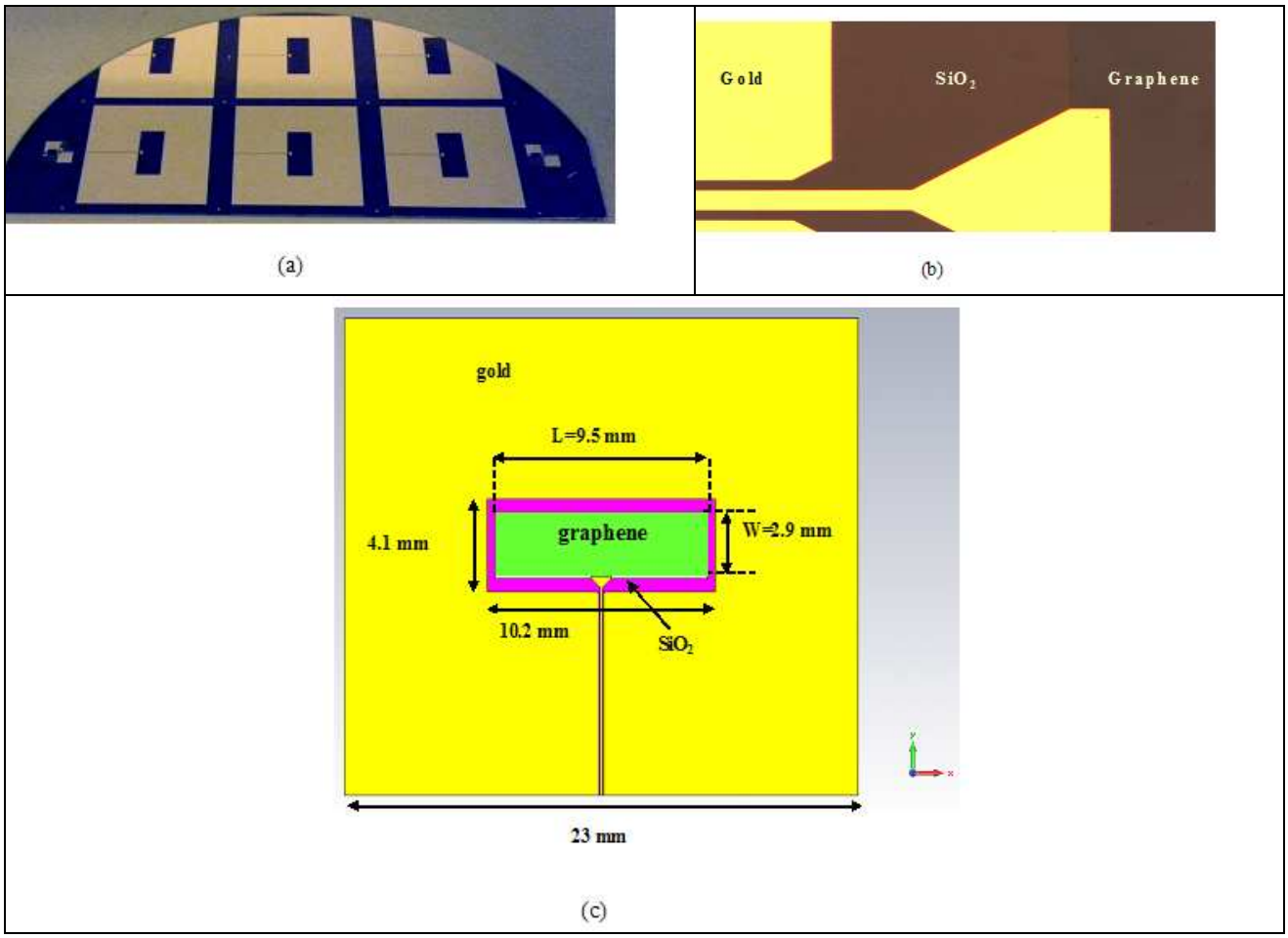


**Figure 17 : The X band graphene antenna**

We have measured the radiation pattern of the antenna which is a difficult task since antenna is very small.
The radiation pattern of the graphene-based antenna was measured using the setup from Fig. 16..

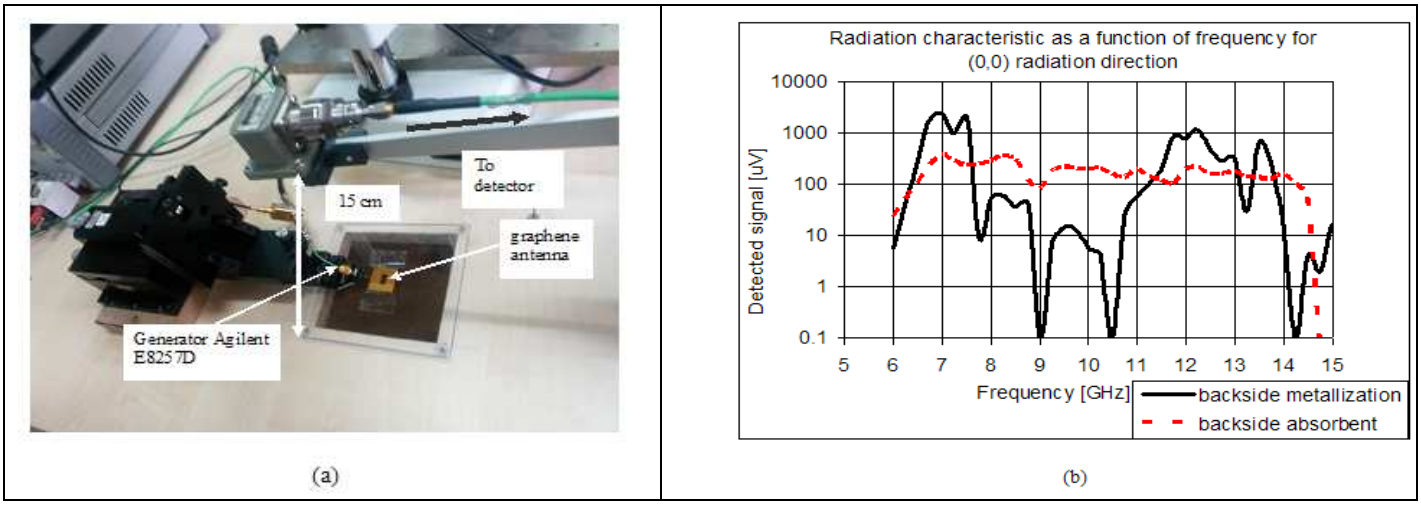


**Figure 18 : (a)** the radiation pattern measurement setup (b) the detected signal as a function of frequency for the radiation direction normal to the antenna plane, for a backside absorbent (dashed trace) and a backside metallization (solid trace).

The antenna under test was contacted on wafer with a G-S-G probe and used as emitter. It was fed by a PSG Analog Signal Generator (Agilent E8257C) with a 6 – 15 GHz microwave signal, modulated in amplitude (10 kHz square AM). A X-band waveguide flange was placed at a distance of 150 mm (satisfying far-field conditions in the X-band) and connected to a 10 MHz – 40 GHz detector (Anritsu). The detected signal is amplified by a SR560 LNA and plotted on an oscilloscope (Tektronix DPO2024). Since the antenna has a thickness of 500 μm, much smaller than the microwave radiation wavelengths which are of the order of few cm at least, the antenna will not radiate only above the radiation plane represented by slots, but also below and thus reducing the radiation efficiency. So we have measured the detected signal at the position (0,0) – perpendicular to the metallization – in two conditions: (i) placing a microwave absorbent on the backside of the antenna (ii) placing metallic surface on the backside of the antenna.

We can see in Fig. 16b that the detected signal in the case the backside metallization is much larger at 7 GHz and 12 GHz while the detected signal in the case of the backside microwave absorbent is more uniform. The 2D radiation patterns in the H-plane (orthogonal to the feed line of the antenna) was recorded at 7 GHz and 12 GHz in the case of the graphene-based antenna with a backside metalized surface (see Fig. 3) and at 8 GHz, 10 GHz and 12 GHz in the case of the graphene-based antenna with a backside absorbent (see Fig. 4). The 3dB beamwidth (when the received power is reduced by half compared to the maximum) is between 40 – 80 degrees for the radiation patterns presented in Fig. 17 and Fig. 18.
In the case of the graphene-based antenna having a backside metallization there are no side lobes at 7 GHz, with one side lobe appearing at 12 GHz meaning that part of the radiated microwave signal travels through the substrate towards the backside metallization and is then reflected back, being added with the frontside radiated signal. For the backside absorbent case, although the effects of the backside radiation are strongly diminished, multiple side lobes appear at 8 GHz and 12 GHz. surface.

In conclusion, we have shown that a graphene-based antenna has unusual properties: the reflection parameter (|S11|) of the antenna is shifted up and down by the DC voltage improving the matching and, in contrast with metallic slot or patch antenna working at the same frequencies, the graphene-based antenna is wideband.

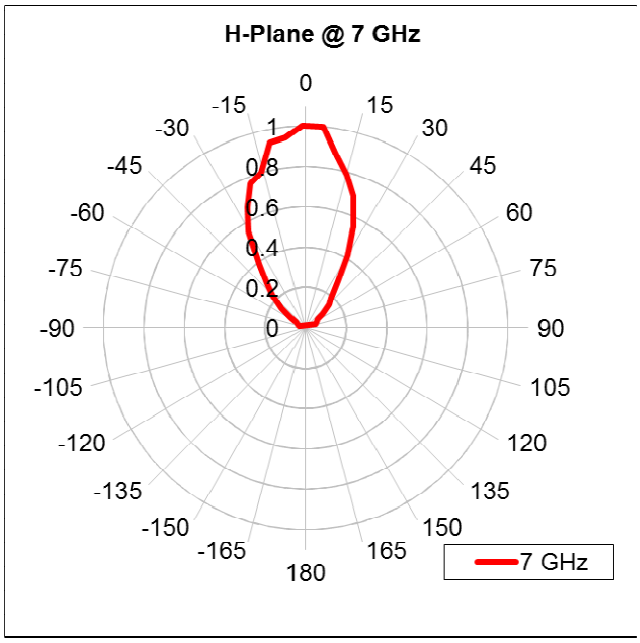


(a)

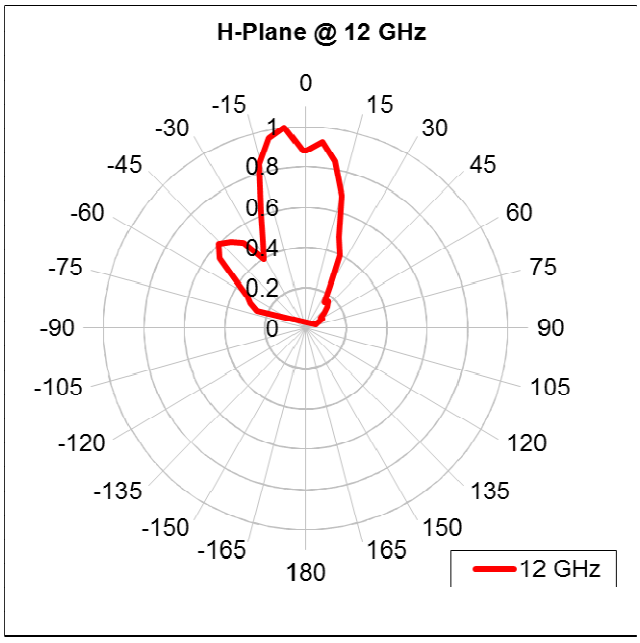


(b)

Fig. 17 The radiation pattern of the graphene-based antenna with a backside metallization normalized at the maximum value, at (a) 7 GHz (b) 12 GHz.

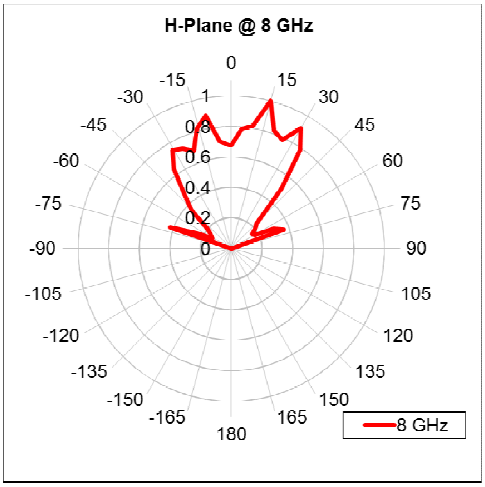


(a)

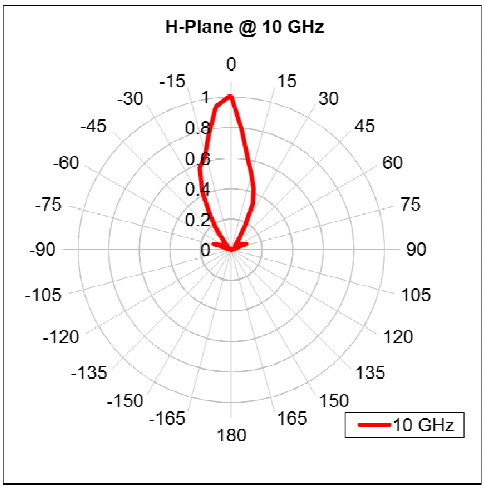


(b)

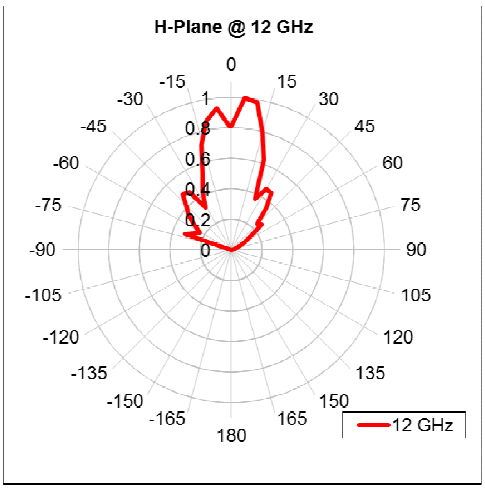


(c)

Fig. 18 The radiation pattern of the graphene-based antenna with a backside metallization normalized at the maximum value, at (a) 7 GHz (b) 12 GHz.

## Nano-RF Publications

In the last 12 months the partners of the Nano-RF project published various results related to the project.

- Publications
    - M. Baldelli, L. Pierantoni, et al., “An educational app for the analysis of the electromagnetic absorption of a graphene multilayer, based on a transmission line model”, submitted to IEEE Microwave Megazine.
    - D. Mencarelli, S. Bellucci, A. Sindona, L. Pierantoni, “Spatial dispersion effects upon local excitation of extrinsic plasmons in graphene micro-discs”, submitted to Physical Review D.
    - D. Mencarelli, A. Sindona, L. Pierantoni, S. Bellucci, “THz-plasmon excitations in graphene micro-discs: ab initio linear response approach vs electromagneic modelling”, submitted to IEEE Transactions on Terahertz Science and Technology.
    - Dragoman, M., Neculoiu, D.,Bunea, A.-C., (...), Pierantoni, L., Modreanu, M., (2015), A tunable microwave slot antenna based on graphene, Applied Physics Letters, 106 (15), 153101, 2015.

- Conference
    - L. Pierantoni, D. Mencarelli, Fabio Coccetti, T. Rozzi “Ballistic Simulation of Ratched effect in antidote lattices partterned on graphene, ” in proceedings of EUMW 2015 6-11 September 2015 - Paris .
    - S. Bellucci, A. Sindona, D. Mencarelli, L. Pierantoni (2015) “Electrical conductivity of graphene: a time-dependent density functional theory study”, Proceedings of the NATO Advanced Research Workshop on Fundamental and Applied NanoElectroMagnetics”, FANEM 2015, Belarus State University, Minsk, Belarus, May 25 – 27, 2015.
    - D. Mencarelli (2015), (invited talk) “Full-wave techniques for the multi-physics modeling and design of nano-structured devices”, Proceedings of the NATO Advanced Research Workshop on Fundamental and Applied NanoElectroMagnetics, FANEM 2015, Belarus State University, Minsk, Belarus, May 25–27, 2015.
    - L. Pierantoni, D. Mencarelli, A. Sindona, M. Gravina, M. Pisarra, C. Vacacela Gomez, S. Bellucci (2015), “Innovative full wave modeling of plasmon propagation in graphene by dielectric permittivity simulations via linear response density functional theory”, Proceedings of the 2015 International Microwave Symposium (IMS), Microwave Symposium Digest (MTT), Phoenix, AZ, USA, May 17–22, 2015.
    - L. Pierantoni, A. Sindona, M. Gravina, M. Pisarra, D. Mencarelli, S. Bellucci (2015), “Comparison of rigorous vs approximate methods for accurate calculation of 2D-materials band structures and applications to THz nanoelectronics”, Proceedings of the 2015 International Microwave Symposium (IMS), Microwave Symposium Digest (MTT), Phoenix, AZ, USA, May 17 – 22, 2015.

# Remember to visit us at:

http://project-nanorf.com/

Nano-RF is a project co-funded by the European
Commission under the FP7 programme
Initiative Advisory Council
Grant Agreement N°: 318352

**Contact:** Dr. Afshin Ziaei, Nano-RF Coordinator,
mailto:afshin.ziaei@thalesgroup.com